Acta Technica *62* (2017), No. 6B, 301–310

Analysis of metal solidification structure evolution based on nonlinear dynamics and statistics

Fushuang Yang[2]

Abstract. In order to improve the analytical precision of metal solidification process, a method of metal solidification process analysis based on cellular automaton decision combination prediction is proposed. Firstly, the temperature field distribution of the alloy solidification process is solved according to the theory of the equivalent heat capacity of heat conduction with phase change; the continuous nucleation model and kinetics model of the dendrite tip growth are combined to conduct coupling simulation for temperature field and grain size organization forming process; secondly, the statistic model of the metal solidification process analysis is built to conduct experimental analysis and obtain the selected value of the optimal clustering coefficient; finally, the validity of the statistical method of the metal solidification process analysis is verified through the simulation experiment.

Key words. Cellular automaton Metal solidification Combination prediction Temperature field Heat conduction with phase change.

1. Introduction

The solidification process of metal is very complicated, generally includes three stages: liquid, solid-liquid two-phase coexistence zone and solid, and in this process, the thermal properties and mechanical properties of the materials are varied greatly. At the same time, the solidification process of metal is not only a process of thermal change, but also a process of microstructure change. Therefore, it is very important to study the deformation behavior and microstructure evolution of metal materials during solidification.

In this paper, the Cu alloy is the object of study and it is a typical solid solution type of dendrite alloy, the phase diagram is complete and the physical properties of the data is complete and accurate, so as to carry out solidification process simula-

[1]College of Mechanical Engineering, Tongling University, Tongling Anhui , 244000, China

tion research. The specific research process is as follows: firstly, the finite element method is used to calculate the temperature field in a certain time step, and then the result is taken as the input file of the grain microstructure simulation program based on the cellular automaton technology to solve the solid fraction value for alloy solidification under the temperature. And then the solid fraction is returned to the finite element, and the temperature field at this time is calculated. This process is repeated and can be used to analyze the coupling between the temperature field and the microstructure evolution process. And then combined with the simulation platform based on VC ++ and the visual programming system, the visualization of grain formation and growth process is realized on the computer. In order to correctly predict the formation of grain in the solidification process, the literature [8] combines the advantages of deterministic methods and probabilistic methods, and proposes a kind of analogue method (i.e. the cellular automaton method) based on the crystal particle nucleation and growth mechanism. This approach captures the main contradiction between simplicity and complexity, thus touching and embodying other contradictions, such as the contradictions among macrocosm and microcosm, definitiveness and randomness, mathematical model and the physical nature, and thus has the capacity to describe the complex, overall, continuous system through the simple local rule and discrete methods.

Based on the above algorithm, a method to analyze the metal solidification process based on the combination of cellular automaton decision combination prediction is proposed in this paper. The temperature field distribution of the alloy solidification process is solved according to the theory of the equivalent heat capacity of heat conduction with phase change; the continuous nucleation model and kinetics model of the dendrite tip growth are combined and the statistic model of the metal solidification process analysis is built to obtain the selected value of the optimal clustering coefficient, so as to realize the efficient analysis of the solidification process.

2. Application of Cellular automaton method in metal solidification simulation

The cellular automaton (CA) method was firstly introduced in the early 1950s by the famous mathematician J V Neumann who is the founder of the computer, in order to simulate the self-replicating function of the life system. The main idea is to divide the ranges to be simulated into several equal-sized, aligned cells, and to disperse the time into a certain interval, and to give all the necessary states of each cell with the necessary information. The state transition of each cell in the forward and backward time steps is determined by a certain evolutionary rule which is throughout all the cells of the system under study. Thus, the state of a cell is affected by the state of the neighbor cell, and also affects the state of the neighbor cell. There is an interaction effect between the localities, and the change of the rule is used to achieve the simulation of the process. With a simple discrete cell to examine complex systems, the cellular automaton is indeed a good way to deal with microscopic evolution.

According to HW Hesselbarth, the following rules should be observed for cellular

automaton: (1) The ranges to be studied or simulated are divided into cell grids with same size and regular arrangement (for two-dimensional, usually quadrilateral or hexagonal) (2) each cell has a definite number of neighbor cells; (3) each cell has a definite state (such as solid state, liquid state, boundary, etc.) and several variable fields (such as temperature field, concentration field, energy field, etc) according to the simulated problems; (4) The evolution rule of a cell in a certain time step is determined by the state and variable of the neighbor cell. The commonly used two-dimensional square cellular automata model consists mainly of the parts shown in Figure%.

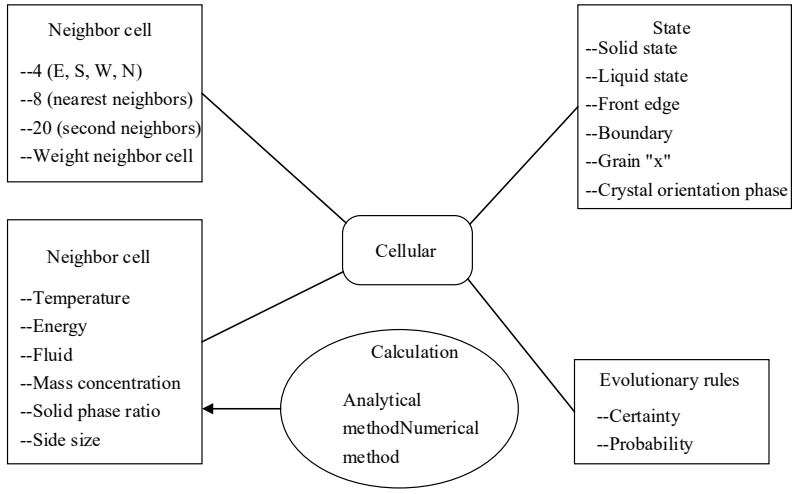

Fig. 1. Composition of cellular automata model

The states and variables of the abovementioned cellular are given a specific value (e.g. 1 for solid state, 2 for liquid, etc), and these values are updated in each time step and the updated data can be calculated as the initial value of the next time step, and the final result can be obtained under such cycle. The evolution rule that controls the change of cellular state is based on the physical metallurgical background of the simulation process, thus determining to a large extent the quality of the model itself, which is also one of the advantages of the cellular automata model (relative to the MC method).

The cellular automaton was originally used in biological systems and subsequently introduced into a wider range of fields such as mathematics, physics, computer and materials science, and now even used in transportation, finance and marketing. The application of cellular automaton in materials science is developed in the past 10 years, and appeared in the solidification and crystallization of cast ingot at the earliest. There is a certain degree of similarity between the solidification of the ingot and the crystallization of welding molten pool. Many theories of the crystallization of welding molten pool are derived from the casting and the important parameters in determining the casting structure, such as temperature gradient, coarsening rate, degree of super-cooling and alloy composition also determines the development of

weld solidification organization. However, it is different to the crystallization of the casting: the welding pool is with small size, solidification speed, and the average cooling rate is about 10000 times than the average cooling rate of steel ingot; the liquid metal in the molten pool is always in a state of overheating, uneven temperature distribution; there are various forces in the welding pool and can be crystallized under the movement condition; the boundary thermal conductivity of the is welding pool also very different with the casting; the solute atoms are distributed uneven during the solidification process and there is segregation phenomenon. All of these have brought considerable difficulty to the simulation of the weld solidification structure.

3. Decision combination prediction

3.1. Decision analysis

For a given metal information data set, the metal space to which the information belongs is R^n, n is the the number of information attributes. The decision classifier DT can divide R^n into Q different ranges, and the categories marks of different ranges r_m are $r_m.cl$. The decision classifier DT is equivalent to the constant segment mapping $f_{DT} : x \to r_m \cdot cl$, which can be used to establish the mapping relationship between the metal information sample $x \in D$ and the corresponding range r_m and obtain the label value $r_m \cdot cl$ in this case.

There are two kinds of expression means of prediction range (r) for constituent component and path structure corresponding to the decision classifier, in which the path structure $(r.p)$ of the prediction range (r) can be described as follows:

$$r.p = \{\cap d(a_v), v = 1, 2, \cdots, K_r\} \ . \tag{1}$$

In the equation (1), $d(a_v)$ is the taking value interval of the range of the metal information attribute (a_v) in the prediction range (r), K_r is the number of nodes involved in the prediction path between the range (r) and the root node, and the operator $(\cap)$ is the intersection of the different attribute quality supervisions. The path structure $(r.p)$ can be used to correlate the decision classifier (DT) and the predicted location range (r), and describes the rule attribute between the range (r) and the root node.

In order to achieve the description of the contents of the metal information set (D) covered in the range (r), the composition structure of (r) is given as follows:

$$r.c = \{num(k_1), num(k_2), \cdots, num(k_J)\} . \tag{2}$$

In the equation (2), J is the number of categories of the metal information set; $num(k_1), num(k_2), \cdots, num(k_J)$ is the number of samples in the range and belongs to different categories of $(k_1, k_2, \cdots, k_J)$. The $r.c$ constituent structure reflects the relationship between the metal information set (D) and the predicted range (r).

For the decision classifier DT_1 and DT_2 with differences in the structure (but have relevance), the similarity description can be carried out based on the affinity

prediction probability, for the metal information prediction probability ($P(r)$), according to the access situation, can be divided into predictive component probability ($P(r.c)$) and prediction path probability ($P(r.p)$), The component of the probability of prediction can be expressed as:

$$P(r_m.p) = V(r_m.p) \Big/ \sum_{l=1}^{Q} V(r_l.p). \tag{3}$$

$$V(r_m.p) = \prod_{v=1}^{K_{r_m}} (|d(a_v)|/|dom(a_v)|). \tag{4}$$

$$P(r_m.c) = |r_m.c| \Big/ \sum_{l=1}^{Q} |r_l.c|. \tag{5}$$

In the above equation, (4) is the super-volume obtained by normalizing the predicted range (r_m) in the metal space (R^n), $|dom(a_v)| = \max(a_v) - \min(a_v)$ represents the interval value of the attribute (a_v), $|d(a_v)| = \max(a_v) - \min(a_v)$ represents the interval value of the metal information attribute (a_v) in the range (r_m). In the equation (13), $|r_m.c| = \sum_{\rho=1}^{J} num(k_\rho)$ represents the sum of all metal information samples in the range (r_m).

The predicted value ($P(r.p)$) of the probability of the path obtained by the equation (4) conforms to the distribution consistency of the attribute. In the case where the training set (D) is accessible, the probability prediction value ($P(r)$) needs to be solved according to equation (5). At the same time, equations (3) and (5) show only the component parts of the predicted probability, and all the probabilistic prediction is calculated as $P(r) = \{P(r_m) | m = 1, 2, \cdots, Q\}$.

After obtaining the probability forecast value ($P(r)$), the similarity expression form of each decision classifier can be obtained based on the following equation:

$$\begin{aligned} S(DT_1, DT_2) &= s(P_{DT1}(r), P_{DT2}(r)) \\ &= \sum_{m=1}^{Q} [P_{DT1}(r_m) \cdot P_{DT2}(r_m)]. \end{aligned} \tag{6}$$

In equation (6), $s(\cdot, \cdot)$ is a probability affinity expression, which can characterize the approximation between different distributions of probabilities and satisfy $0 < s(\cdot, \cdot) < 1$. Then, the $S(DT_1, DT_2)$ value interval is also $(0, 1]$. For the DT_1 and DT_2 with higher similarity to the predicted probability, $S(DT_1, DT_2)$ value is close to the upper limit 1, otherwise the $S(DT_1, DT_2)$ value is closer to the lower limit 0. If $P_{DT1}(r) = P_{DT2}(r)$ exists, then it is available.

The fraction decision calculation process is as follows:

Step1: (prior knowledge) uses the data set (S_i) in the original data field of the metal information to train the decision classifier (DT_i) and train the target decision classifier (DT_i) with the target domain metal information set (T).

Step2: The similarity determination in turns between the decision classifier (DT_i)

and the metal target information (DT_i) is conducted to obtain $S(DT_T, DT_i)$. If the data set (S_i) in the original data field of the metal information can be accessed, the component structure ($r.c$) in the metal information area (r) can be predicted based on the equation (10), and the probability value ($P(r.c)$) of the predicted component is obtained by combining equation (13). Otherwise the path structure ($r.p$) can be obtained based on equation (13), and then the probability ($P(r.p)$) of the predicted path probability can be obtained by combining equation (15).

Step3: The similarity ($S_i(DT_T, DT_i)$) of different metal targets is normalized and the weight values (ω_i) are obtained, and the decision classifier is allocated.

Step4: The fraction decision classifier ($DT_T = \sum_{i=1}^{N} \omega_i DT_i$) is obtained based on the linear combination and the fraction decision value is output.

3.2. Fractional correction

All metal information in the training set can be extracted to a temperature list, and these temperatures are used to represent a model. Since the number of temperatures in the metal information is different, the interpolation function can be used in each mode to scale the metal information in the training set to the maximum possible. Then, a vector space representation can be constructed, where each dimension represents one of the matching patterns. In the emotional method model score prediction, the decision classifier shown in section 3.1 is used to carry out the metal information fraction prediction training.

Example 5: The metal information t_k is given. In this example, we extract the temperature list and their respective fraction: <some, -0.20>, <instagram, -0.20>, <photos, 0.05>, <just, -0.77>, <so, -0.60>, <funny, -0.19>, <# sarcasm, -2.35>. Figure 3 shows the pattern of the above data. In our training set, the maximum number of temperatures that can be extracted from the metal information is 24.

The content-based approach and the emotion-based modules of combination metal information are evaluated as follows:

$$S = \alpha \times SC + \beta \times SE\,. \tag{7}$$

Where, S is the final score of the metal information. SC is the metal information score calculated by the content-based method module and SE is the metal information score calculated based on the emotion-based method module. α and β are the weight coefficients based on the training error scores of each method's classification model, and $\alpha + \beta = 1$.

4. Experiment analysis

4.1. Material parameters

The density of the thermophysical property material of the metallic prefabricated body is 4.47 × 103kg; the specific heat capacity is 260J/kg°; the thermal conductivity is 14.23 W/m·°; the phase change of the aluminum alloy has the melting

point of 696°kg/m^3; the specific heat under the solid phase is 896J/kg°; the specific heat under the liquid phase is 1050J/kg°; latent heat is 3956440J/kg. The thermal properties parameters of the aluminum alloy and the prefabricated body used in the experiment are shown in Table 1.

Table 1. Mechanical properties of aluminum alloy and prefabricated body

	Elasticity modulus	Expansion factor	Poisson's ratio
Aluminum alloy	73.1	23.1	0.34
Prefabricated body	426	4.7	0.18

4.2. Calculation of macro-temperature field in solidification process

Figure 2 shows the change of the temperature of the points of the casting in the Z direction in the solidification process with time. It can be seen from the figure that the temperature drop at the point near the runner mouth is gentler and there is a clear platform because the alloy is far from the boundary and the heat dissipation is less and the latent heat of the alloy is released when it is solidified. On the contrary, the cooling rate is fast when closes to the cold iron, and no latent heat phenomenon occurs, no platform phenomenon, which shows the cooling rate of the alloy along the Z direction is different.

Figure 3 shows the calculation results of the cooling curves at two points (Z = 148mm and Z = 20mm) in the Z direction. The results show that the two methods are in good line with each other, indicating that the calculation method is correct and feasible. The author believes that the error occurred may be due to the incorrect readings produced in the process of the thermocouple temperature measurement, and the maximum error is only 4.7%, which meets the general engineering requirements.

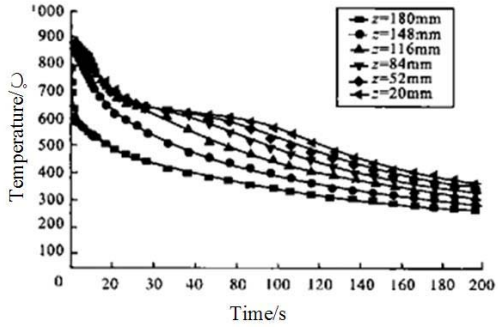

Fig. 2. Variation rule of temperature of points of the casting in the Z direction

Figure 4 shows the change of the temperature of the prefabricated body and molten metal in the pores at different nodes during the solidification process. In the prefabricated body, the nodes on the matrix boundary at the initial cooling stage are cooled rapidly, as shown in node I in the figure, while the nodes II and III are cooled slowly since they are far away from the boundary. The internal nodes start

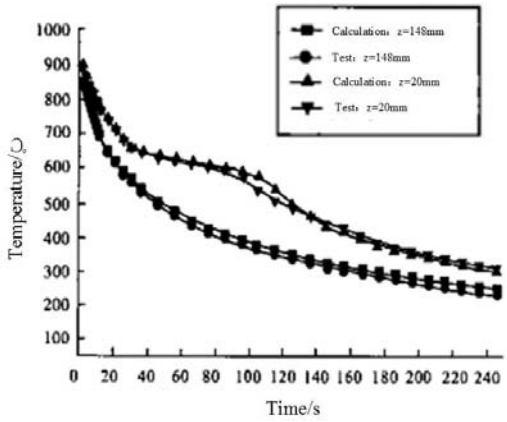

Fig. 3. Comparison of the calculated results with the measured results

to accelerate with the decrease of the temperature of the peripheral nodes. The time shown in the figure is from 200s due to the previous non-pressure infiltration process, the solidification process immediately is conducted after the infiltration process, and here only gives the temperature changes of the solidification process. For the molten metal in the pores, the node I contacts the boundary matrix and begins to cool down after the boundary matrix begins to cool down for a period, and the cooling rate is accelerate; node II and III are in the enter of the pores and not in contact with the matrix, and the cooling rate is slow. The cooling temperature reaches 600° at 750s, and the whole model is basically solidified; when it reaches 400 °, it begins to cool slowly and basically reaches insulation state.

When the high-temperature liquid alloy is injected into the prefabricated body, the material interface is to withstand a huge thermal shock and the temperature is increased, and it is too late to transfer heat, and to withstand compressive stress along the wall thickness in the existence of a certain temperature gradient. The temperature rise of the preset outer boundary is slow and bears the tensile stress. If the heat dissipation is not sufficient, it is easy to crack under the actions of the compressive and tensile stresses. Figure 5 shows the change chart of the prestressing force of the material interface nodes at different solidification times. It can be found that the amount of stress released increases and is non-linearly increased as the settling time increases.

5. Conclusion

In this paper, a metal solidification process analysis method based on cellular automata decision combination is proposed to solve the temperature field distribution of the alloy solidification process. The coupling simulation between the temperature field and the grain formation process is carried out to construct the statistical model of metal solidification process analysis. The validity of the statistical method of the metal solidification process analysis is verified by the simulation experiment.

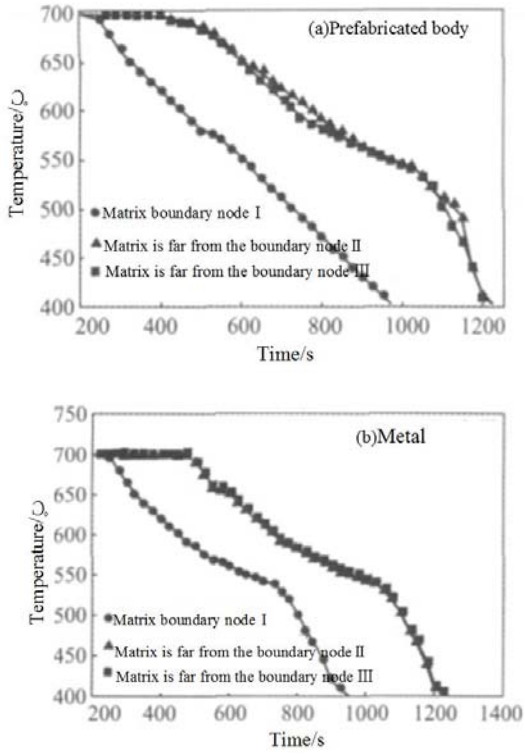

Fig. 4. The Curve of temperature variation of different nodes in solidification

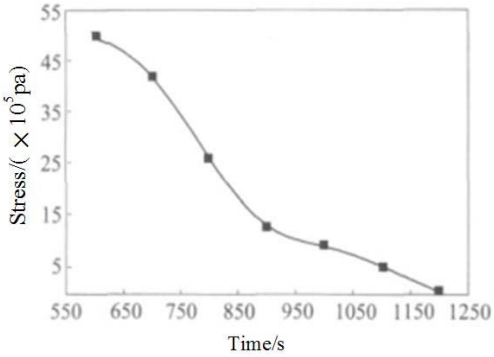

Fig. 5. The value of prestressing force at the interface of the material changes with time

According to the analysis results, the alloy solidification process is consistent with the following phenomena:

(1) In the early stage of cooling, the internal nodes are slowly to cool since they are far away from the boundary, and the cooling rate of the internal nodes starts to accelerate as the temperature of the peripheral nodes decreases.

(2) Due to different thermal expansion coefficient and heat release capacity, the stress concentration is most likely to occur at the interface of the material.

Acknowledgement

The Key Project of Science Research in Colleges and Universities of Anhui Province(No. KJ2016A706).

References

[1] Nastac L: (2011) *Mathematical Modeling of the Solidification Structure Evolution in the Presence of Ultrasonic Stirring*[J]. Metallurgical and Materials Transactions B, 42(6):1297-1305.

[2] Liu R, Dong K, Liu F, et al.: (2005) *Formation and evolution mechanisms of large-clusters during rapid solidification process of liquid metal Al*[J]. Science China Physics, Mechanics & Astronomy, 48(1):101-112.

[3] Yuan Y Q, Zeng X G, Chen H Y, et al.: (2013) *Molecular dynamics simulation on microstructure evolution during solidification of copper nanoparticles*[J]. Journal of the Korean Physical Society, 62(11):1645-1651.

[4] Zhang X L, Zhou Y Z, Jin T, et al.: (2013) *Effect of Solidification Rate on Grain Structure Evolution During Directional Solidification of a Ni-based Superalloy*[J]. Journal of Materials Science & Technology, 29(9):879-883.

[5] Pan D, Xu Q Y, Liu B C: (2010) *Modeling of Mircrostructure Evolution in Directional Solidification of Ni-Based Superalloy Turbine Blade*[J]. International Journal of Gynecological Cancer Official Journal of the International Gynecological Cancer Society, 97-101(5):3207-3210.

[6] Krzesinski J M: (2005) *Numerical Simulation of Grain Structure Evolution in Solidification of an Al-5.0wt%Cu Alloy under Electromagnetic Stirring and Its Experimental Verification*[J]. Isij International, 45(2):183-191.

[7] Ogborn J S, Olson D L, Cieslak M J: (1995) *Influence of solidification on the microstructural evolution of nickel base weld metal*[J]. Materials Science & Engineering A, 203(1):134-139.

[8] Terasaki H, Komizo Y, Yonemuira M, et al.: (2006) *Time-resolved in-situ, analysis of phase evolution for the directional solidification of carbon steel weld metal*[J]. Metallurgical and Materials Transactions A, 37(4):1261-1266.

[9] Yue T M, Li T: (2007) *Solidification Behaviour and the Evolution of Microstructure in the Laser Cladding of Aluminium on Magnesium Substrate*[J]. Materials Transactions, 48(5):1064-1069.

[10] Ma X, Li D: (2015) *Non-equilibrium Solidification and Microsegregation Mechanism Based on Interface Evolution and Discrete Crystal Growth*[J]. Metallurgical and Materials Transactions A, 46(2):549-555.

[11] Peng H, Zhilong Z, Jiandong T, et al.: (2010) *Microstructural evolution of directional solidification aluminum alloy under high intensity pulsed current*[J]. Special Casting & Nonferrous Alloys, 30(5):450-452.

[12] Kluska-Nawarecka S, Smolarek-Grzyb A, Byrski A, et al.: (2008) *Optimization of simulation model parameters for solidification of metals with use of agent-based evolutionary algorithm*[J]. Computer Science, 9(Suppl 2):76-8.

Received May 7, 2017